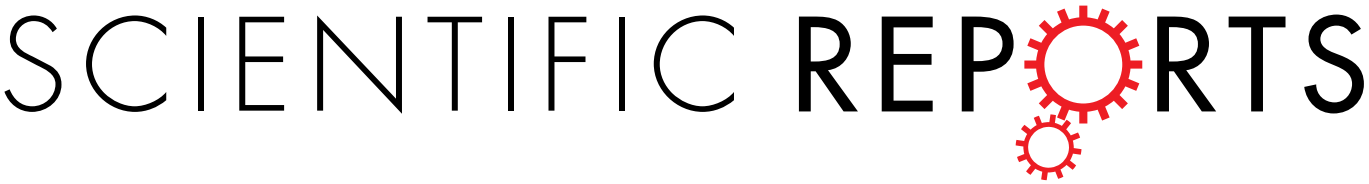

OPEN

Kondo peak splitting and Kondo dip induced by a local moment

Pengbin Niu[1,5], Yun-Long Shi[1], Zhu Sun[1], Yi-Hang Nie[2] & Hong-Gang Luo[3,4]

Received: 16 June 2015
Accepted: 10 November 2015
Published: 10 December 2015

Many features like spin-orbit coupling, bias and magnetic fields applied, and so on, can strongly influence the Kondo effect. One of the consequences is Kondo peak splitting. However, Kondo peak splitting led by a local moment has not been investigated systematically. In this research we study theoretically electronic transport through a single-level quantum dot exchange coupled to a local magnetic moment in the Kondo regime. We focus on the Kondo peak splitting induced by an *anisotropic* exchange coupling between the quantum dot and the local moment, which shows *rich* splitting behavior. We consider the cases of a local moment with $S=1/2$ and $S=1$. The longitudinal (z-component) coupling plays a role of multivalued magnetic fields and the transverse (x, y-components) coupling lifts the degeneracy of the quantum dot, both of which account for the fine Kondo peak splitting structures. The inter-level or intra-level transition processes are identified in detail. Moreover, we find a Kondo dip at the Fermi level under the proper parameters. The possible experimental observations of these theoretical results should deepen our understanding of Kondo physics.

The Kondo effect[1–3], first discovered experimentally in the 1930's as an anomalous increase in the resistance of metals containing magnetic impurities, is a many-body phenomenon. In an electronic transport setup, the Kondo effect can also be realized in quantum dots strongly coupled to external leads[4]. Physically, the higher-order virtual tunneling events can effectively flip and hence screen the local spin on the dot, thus the electrons in the leads and on the dot together form a spin-singlet state. This macroscopically correlated state produces a narrow peak in the dot's density of states (DOS) around the Fermi level and is known as the spin Kondo effect.

Some recent progress has focused on Kondo peak splitting, which may deepen and enrich our understanding of Kondo effects. Kondo peak splittings may be induced by external factors[5–8]. In particular, external bias and magnetic field may lead to the Kondo peak splitting[5]. The zero-bias peak splits with external bias voltage, since Kondo resonance is pinned to the Fermi level of each lead. A magnetic field splits the one Kondo peak by the Zeeman effect because that dot's spin-degenerate energy levels split into separate spin-opposite levels. Moreover, when external ferromagnetic leads are involved, a parallel alignment splits the zero-bias anomaly even in the absence of an external magnetic field, and an antiparallel spin alignment splits Kondo peaks only in the presence of a magnetic field[6,7]. Interestingly enough, the valley degree of freedom of external leads reveals a zero-Zeeman-field valley splitting and shows strong temperature dependence, as recently observed in experiments[8].

Naturally, Kondo peak splittings may also appear when an additional degree of freedom appears[9–26], such as an orbital degree of freedom (the orbital Kondo effect)[9] or another spin degree of freedom. In carbon nanotube quantum dots with spin-orbit coupling[10], splittings emerge when the spin and orbital degrees of freedom couple each other, lift the fourfold degeneracy of a single electron in the dot, and break the SU(4) symmetry[11]. When another spin degree of freedom is involved, such as the large spin of single molecular magnets, a local spin-half impurity, or a magnetic cluster[12–26], Kondo peak splittings could occur. In single molecular magnets, the magnetic anisotropy of local large spin acts like a magnetic field[24]. In a quantum dot with spin-half impurity, a three-peak Kondo structure characterizes the isotropic exchange interaction between the dot electron and impurity[25]. Finally, in magnetic cluster experiments, a Kondo peak on a Co adatom can be split when the atom interacts with a magnetic Fe cluster. This splitting, depending on the adsorption site, is demonstrated by reversible switching of an adatom between two positions[26].

[1]Institute of Solid State Physics and Department of Physics, Shanxi Datong University, Datong 037009, China. [2]Institute of Theoretical Physics, Shanxi University, Taiyuan 030006, China. [3]Center for Interdisciplinary Studies & Key Laboratory for Magnetism and Magnetic Materials of the MoE, Lanzhou University, Lanzhou 730000, China. [4]Beijing Computational Science Research Center, Beijing 100084, China. [5]Shanxi Provincial Key Laboratory of microstructural electromagnetic functional materials, Datong 037009, China. Correspondence and requests for materials should be addressed to P.N. (email: 120233951@qq.com)

We consider theoretically the Kondo peak splitting phenomenon in electronic transport through a single level quantum dot exchange coupled to a local moment, mainly focusing on an anisotropic coupling. Despite the fact that the relevant aspects of the Kondo effect have been widely studied in many models, for example, the T-shaped double quantum dot or two-impurity Kondo problems[27–33], the anisotropic exchange coupling between two spin degrees of freedom and its impact on the Kondo effect have not to be explored in detail. One of the challenges of this study is that we have to deal with two anisotropy couplings: the longitudinal anisotropy coupling $J_{\parallel}$ and the transverse anisotropy coupling $J_{\perp}$. In the limiting case of strong longitudinal anisotropy coupling, the local moment behaves like a multi-valued quantum magnetic field, and in the isotropic coupling limit, the results show a three-peak Kondo structure consistent with ref. 25. In the general anisotropic case, the degeneracy is lifted and we can identify the entangled states via which Kondo transport occur. The inter-level or intra-level transitions are also identified, which account for the fine Kondo-peak-splitting structures. Moreover, we find a Kondo dip at the Fermi level under proper parameters. To evaluate the dot's density of states and differential conductance, we use a non-equilibrium Hubbard operator Green's function method[34]. To calculate the relevant Hubbard operator Green's functions from the equations of motion, we apply the truncation scheme introduced in ref. 5.

Results

Hamiltonian. We consider a model consisting of a single level (SL) quantum dot exchange coupled to a local magnetic moment (spin S). This model may be realized in some systems, for instance, magnetic adatoms coupled to a magnetic cluster, quantum dots coupled to a localized magnetic impurity, or a CdTe quantum dot doped with a single metal ion[35–41]. The exchange coupling is anisotropic and the total Hamiltonian of this model consists of three terms, $H = H_{Leads} + H_D + H_T$, in which

$$\begin{aligned} H_{Leads} &= \sum_{k,\alpha,\sigma} \varepsilon_{k\alpha} c^{\dagger}_{k\alpha\sigma} c_{k\alpha\sigma}, \\ H_D &= \varepsilon_0(\hat{n}_{\uparrow} + \hat{n}_{\downarrow}) + U\hat{n}_{\uparrow}\hat{n}_{\downarrow} - J_{\parallel} s^z S^z - \frac{J_{\perp}}{2} s^{+} S^{-} - \frac{J_{\perp}}{2} s^{-} S^{+}, \\ H_T &= \sum_{k,\alpha,\sigma} (t_{k\alpha} c^{\dagger}_{k\alpha\sigma} c_{\sigma} + H.c.). \end{aligned} \tag{1}$$

H_{Leads} is the Hamiltonian of the electrodes, where $\varepsilon_{k\alpha}$ is the energy for free electrons, with $\alpha = L, R$ enumerating left and right leads, and $c^{\dagger}_{k\alpha\sigma}$ ($c_{k\alpha\sigma}$) are electronic creation (annihilation) operators in the electrodes, with $\sigma = \uparrow, \downarrow$ representing the up and down electron spins. H_D is the Hamiltonian of the dot, where ε_0 is the SL energy of the dot and U is the Coulomb interaction strength, with $\hat{n}_{\sigma} = c^{\dagger}_{\sigma} c_{\sigma}$ the number operator. $c^{\dagger}_{\sigma}$ and c_{σ} are electronic creation and annihilation operators on the SL in the dot. We consider in the calculation below the limit of infinite Coulomb interaction ($U \to \infty$), thus only one electron is allowed to occupy the SL. S^z is the z-component of the local spin and s^z is the spin of the electron in the SL. The corresponding operators $S^{\pm}(s^{\pm})$ are the ladder operators. $J_{\parallel} = \beta J$ is the z-axis exchange coupling between the local spin and SL, and $J_{\perp} = \alpha J$ is the x-y plane exchange coupling, where α is the transverse anisotropy parameter and β the longitudinal anisotropy parameter. We consider ferromagnetic coupling ($J > 0$) and $\alpha, \beta \in [0, 1]$. We expect that the transverse and longitudinal terms in Eq. (1) has different splitting effects on Kondo transport when they appear separately, while they have a combined effect when both terms appear. Thus, there are three limiting cases in our model: i) $\beta = 1$ and $\alpha = 0$, the strong longitudinal anisotropy coupling case; ii) $\beta = 0$ and $\alpha = 1$, the strong transverse anisotropy coupling case; and iii) $\beta = 1$ and $\alpha = 1$, the isotropic coupling case. H_T is the tunnel Hamiltonian between the leads and dot, where $t_{k\alpha}$ are the tunneling amplitudes. The Hamiltonian H_D is easily diagonalized. In the results and discussions, we will restrict our calculations to the cases of local spin with $S = 1/2$ and $S = 1$, which are the smallest non-trivial values. For $S = 1/2$, two electrons entangle each other, but with an anisotropic exchange coupling. Thus it is worthwhile to provide explicitly the dot's eigenstates and eigenvalues. The eigenstates and eigenvalues are easily obtained. $|1,0\rangle^{-} = \frac{1}{\sqrt{2}}(|\uparrow\downarrow\rangle + |\downarrow\uparrow\rangle)$ is a spin triplet state, with energy $\varepsilon^{-}(1,0) = \varepsilon_0 + J_{\parallel}/4 - J_{\perp}/2$, and $|\uparrow\uparrow\rangle$ and $|\downarrow\downarrow\rangle$ are the other two triplet states, with energy $\varepsilon_0 - J_{\parallel}/4$. The degeneracy of these triplet states will be lifted in the general anisotropic coupling case. $|1,0\rangle^{+} = \frac{1}{\sqrt{2}}(|\uparrow\downarrow\rangle - |\downarrow\uparrow\rangle)$ is the spin singlet state with energy $\varepsilon^{+}(1,0) = \varepsilon_0 + J_{\parallel}/4 + J_{\perp}/2$.

Splitting behaviors for $S = 1/2$. We now present the Kondo peak splitting effects induced by the longitudinal and transverse anisotropy couplings. Experimentally, the low-temperature differential conductance dI/dV near zero source-drain bias directly reflects the Kondo features in the dot density of states $\rho_{\sigma}(\omega) = (-1/\pi) Im G^{r}_{\sigma}(\omega)$. Within the Keldysh formalism[42,43], the transport current is $I = (e/h)(\Gamma_L \Gamma_R/\Gamma) \sum_{\sigma} \int d\omega [f_L(\omega) - f_R(\omega)](-Im G^{r}_{\sigma}(\omega))$. In the numerical results presented below, we assume symmetric dot-lead couplings $\Gamma_L = \Gamma_R$ and a symmetrically applied source-drain bias ($\mu_L = V/2$, $\mu_R = -V/2$). The energy unit is taken as $\Gamma = \Gamma_L + \Gamma_R = 1$. Since the presence of the Kondo resonance and its possible splitting play an important role in the transport, it is helpful to first estimate the Kondo temperature T_K, which can be calculated from the half width at half maximum of the Kondo resonance[44–46]. For the parameters used in Fig. 1, one gets $T_K/\Gamma \approx 0.026$.

Figures 1 and 2 show the splitting effects of the anisotropy parameters α and β for the minimal non-trivial spin $S = 1/2$. Figure 1 shows the differential conductance, related energy spectrum, and three transition processes. Figure 1(a) shows the differential conductance with a gradual transverse anisotropy parameter, from $\alpha = 0$ to $\alpha = 1$, and fixed longitudinal parameter $\beta = 1$, in which we can clearly observe the Kondo peak splitting effects. In Fig. 1(b), we present the energy spectrum of H_D and the corresponding eigenstates, which have been calculated in section II.

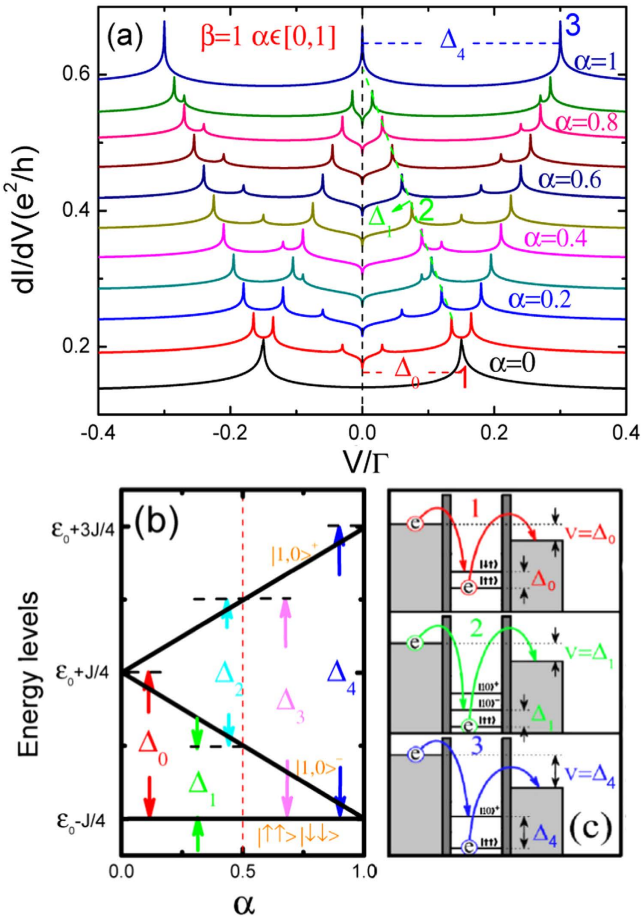

Figure 1. (**a**) dI/dV versus V with fixed longitudinal parameter $\beta = 1$ and gradual transverse anisotropy parameter, from $\alpha = 0$ to $\alpha = 1$, with $\delta\alpha = 0.1$ from the bottom up for each curve. The curves for $\alpha \neq 0$ are shifted upward for clarity. The parameters used are $S = 1/2$, $\varepsilon_0 = -3$, $J = 0.3$, $T = 0.0001$, and the high-energy cutoff $W = 1000$. Δ_0(red), Δ_1(green) and Δ_4(blue) are level spacings corresponding to peaks marked by the numbers 1, 2, and 3. The energy unit is taken as $\Gamma = \Gamma_L + \Gamma_R = 1$. (**b**) The energy spectrum of H_D as a function of the transverse anisotropy parameter α. Δ_i ($i = 0, 1, 2, 3, 4$) are inter-level energy differences. (**c**) Schematic representation of three transition processes producing the peaks marked 1, 2, and 3 in (**a**).

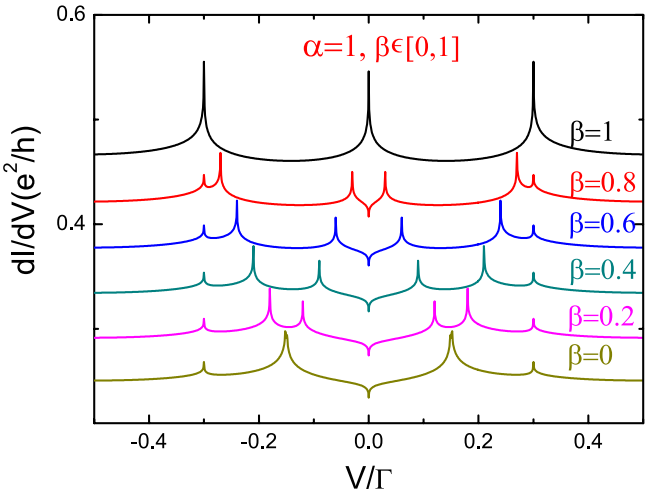

Figure 2. Differential conductance dI/dV with fixed transverse anisotropy parameter $\alpha = 1$ and gradual longitudinal parameter, from $\beta = 0$ to $\beta = 1$, as a function of bias voltage. The curves for $\beta \neq 0$ are shifted upward for clarity, the same as in Fig. 1. The parameters are chosen as $S = 1/2$, $\varepsilon_0 = -3$, $J = 0.3$, $T = 0.0001$, and $W = 1000$. Energy is measured in Γ.

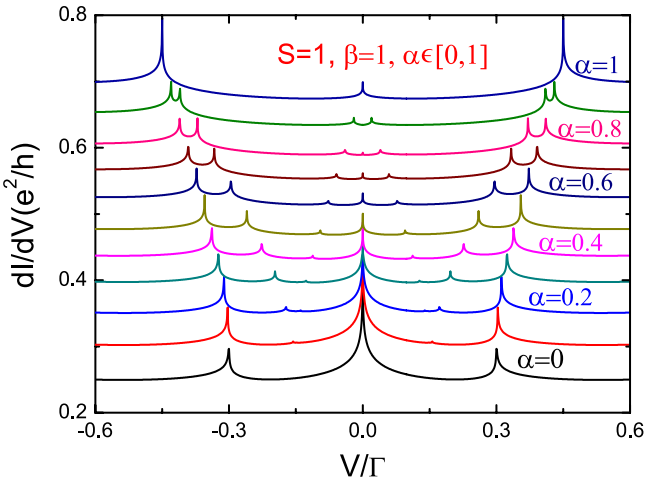

Figure 3. Differential conductance *dI*/*dV* with fixed longitudinal parameter and gradual transverse parameter as a function of bias voltage for $S=1$. The parameters are chosen as $\varepsilon_0=-3$, $J=0.3$, $T=0.0001$, and $W=1000$. Energy is measured in Γ.

Accordingly, we also get five energy level differences, $\Delta_0=\pm J/2$, $\Delta_1=\pm\ (J_\parallel-J_\perp)/2=\pm J(1-\alpha)/2$, $\Delta_2=\pm J_\perp=\pm\alpha J$, $\Delta_3=\pm(J_\parallel+J_\perp)=\pm J(1+\alpha)/2$, and $\Delta_4=\pm J$, which are shown in Fig. 1(b).

Without the local moment ($J=0$), the Kondo singlet state transporting through the SL quantum dot manifests itself as a well-known single sharp peak at $V=0$ in conductance. For the strong longitudinal anisotropy case ($\beta=1$ and $\alpha=0$), the effect of the local moment is equivalent to a magnetic field. The dot's single level $|\Psi\rangle=\alpha|\uparrow\rangle+\beta|\downarrow\rangle$ is now coupled with a " Zeeman field" S^z and split into two energy levels $|\uparrow\downarrow\rangle(|\downarrow\uparrow\rangle)$ and $|\downarrow\downarrow\rangle$ $(|\uparrow\uparrow\rangle)$, as seen in Fig. 1(b), at $\alpha=0$. This mechanism is similar to magnetic field induced Kondo peak splitting[5]. The Kondo singlet state tunneling through the dot is a virtual spin-flip process, and thus only inter-level transitions are allowed, which explains the two peaks with $\alpha=0$ in Fig. 1(a) and why there is no peak at the Fermi surface ($V=0$). However, the magnetic field here is a "quantum" one, and it can take two values with $\hbar/2$ and $-\hbar/2$, which are degenerate.

When we turn on the transverse anisotropy parameter α, i.e., the term $(J_\perp/2)s^+S^-+(J_\perp/2)s^-S^+$, the degeneracy is lifted. In fact, there are two effects of $(J_\perp/2)s^+S^-+(J_\perp/2)s^-S^+$: it i) entangles the states $|\uparrow\downarrow\rangle$ and $|\downarrow\uparrow\rangle$ and ii) lifts the degeneracy of $|\uparrow\downarrow\rangle$ and $|\downarrow\uparrow\rangle$ and splits the dot's energy level. For $0<\alpha<1$, there are seven peaks observed in Fig. 1(a). This splitting, originating from the dot's energy level splitting, can be explained with energy level differences. When Kondo transport occurs, it can happen via inter-level transitions or intra-level transitions [see schematic representation of three transitions in Fig. 1(c)]. $\Delta_i(i=1,2,3)$ correspond to six inter-level transitions, and the peak at $V=0$ corresponds to intra-level transitions. Thus, there are seven peaks observed. Specifically, when $\alpha\neq0$, three separated states form: $|10\rangle^+$,$|10\rangle^-$, and the fully polarized state $|\uparrow\uparrow\rangle$ or $|\downarrow\downarrow\rangle$. Kondo transport occurs via either one or two of these states. For example, the intra-level transition $|10\rangle^+\leftrightarrow|10\rangle^+$ or $|10\rangle^-\leftrightarrow|10\rangle^-$ induce the Kondo peak at $V=0$ and the inter-level transitions $|10\rangle^-\leftrightarrow|\uparrow\uparrow\rangle$ induce the Kondo peaks at $V=\pm\Delta_1$. It seems that the position of the peak at $V=0$ is the same as for a single-level quantum dot, but the underlying mechanism is different. The former is a two-electron entangled state, while the latter is a one-electron state.

When $\alpha=1$, the exchange coupling becomes isotropic. This isotropic interaction induces a three-peak structure. This structure is also observed in spin-orbit coupling[11], which can be formulated as $J_{SO}\overrightarrow{s}\cdot\overrightarrow{l}$. When the anisotropic interaction develops into an isotropic one, one observes that the number of Kondo peaks is reduced. This is because the entangled state $|10\rangle^-$ becomes degenerate with the fully polarized states [see Fig. 1(b)].

We now focus on the strong transverse anisotropy coupling case ($\beta=0$ and $\alpha=1$), which is shown in Fig. 2. In Fig. 2 we present the results with a gradual longitudinal anisotropy parameter, from $\beta=0$ to $\beta=1$, with fixed transverse parameter $\alpha=1$. For $0<\beta<1$, there are also seven peaks observed, which confirm the result in Fig. 1(a). For $\beta=0$, we observe five Kondo peaks, which are located at $V=0$, $\pm J_\perp/2$ and $\pm J_\perp$. These five peaks may also be explained by using the language of intra- and inter-level transitions.

Splitting behaviors for $S=1$. Up to now, we have studied the conductance diagram of the system as a function of the anisotropy parameters for $S=1/2$. However, for a given magnetic cluster or molecule, the local spin usually has the value $S>1/2$. Here, we restrict our discussion to the case of a spin $S=1$. We will study the behavior of the conductance varying the anisotropy parameters. The goal is to understand how the values of the local spin influence the behavior of the conductance and Kondo peak splittings.

Figures 3 and 4 present the differential conductance for integer spin $S=1$. As with $S=1/2$, we vary one of the anisotropy parameters while the other one remains fixed. As seen in Fig. 3, when $\beta=1$ and $0<\alpha<1$, seven peaks are still observed. This is because the energy levels are split into three as before, and are enumerated as $\varepsilon^+(1,\pm1/2)$, $\varepsilon^-(1,\pm1/2)$, and the fully polarized states $\varepsilon(\uparrow,S)$. However, one can deduce that when S grows greater, energy levels increase, and likewise with energy level differences and Kondo peaks. When $\beta=1$ and $\alpha=0$, one has the

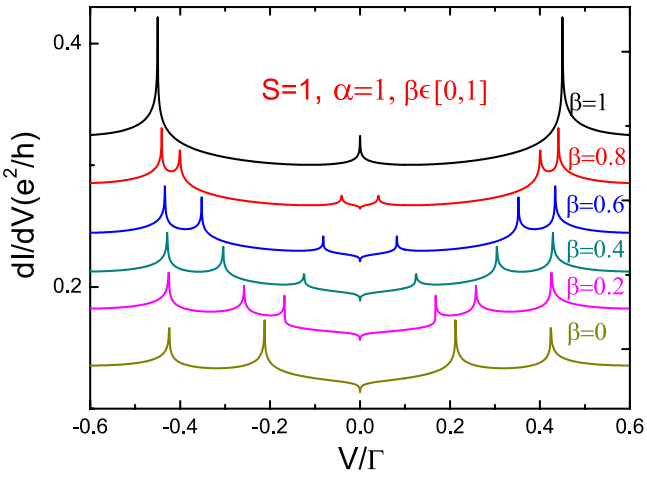

Figure 4. Differential conductance *dI*/*dV* with fixed transverse parameter and gradual longitudinal parameter as a function of bias voltage for $S=1$. The other parameters are the same as in Fig. 3. Energy is measured in Γ.

strong longitudinal anisotropy case. In this situation, the quantum magnetic field S^z takes three values, $-\hbar$, $\hbar$, and 0. As a result, at $V=\pm J$ there are two peaks corresponding to inter-level transitions and for $S^z=0$ it is equivalent to a zero-Zeeman-field corresponding to the Kondo peak at $V=0$. For the strong transverse anisotropic case ($\beta=0$ and $\alpha=1$), we observe five peaks, which are located at $V=0$, $\pm\sqrt{2}J_\perp/2$ and $\pm\sqrt{2}J_\perp$, as seen in Fig. 4. In Figs 1–4, one can observe a Kondo dip at the Fermi surface ($V=0$). This dip is a feature of anisotropic coupling. Under proper parameters, the anisotropic coupling will change the sign of Kondo self-energy at $V=0$ and induce the Kondo dip. Moreover, one can conclude that the interplay of $J_\parallel$, $J_\perp$, and temperature can strongly influence the Kondo resonance at the Fermi surface, i.e., the formation or destruction of a Kondo peak (dip) at Fermi surface.

Methods

The non-equilibrium Green's function method has been widely used in the discussion of Kondo effects in quantum dots[5,47–51]. In order to handle the large spin involved in many problems, we use the Hubbard operator Green's function method[34], which has been used to solve the transport problems in the linear response, non-linear response, and Kondo regimes[52–54]. In this Hubbard operator representation, the electron operators in the dot are rewritten as $c_\sigma = X^{0\sigma} + \delta_\sigma X^{\bar{\sigma}2}$ with $\delta_\sigma=+1(-1)$ for $\sigma=\uparrow(\downarrow)$, $s^z=\frac{1}{2}(X^{\uparrow\uparrow}-X^{\downarrow\downarrow})$, $s^+=X^{\uparrow\downarrow}$ and $s^-=X^{\downarrow\uparrow}$. In the limit of infinite Coulomb interaction ($U\to\infty$), double-occupation is forbidden and $c_\sigma=X^{0\sigma}$. The large spin operators can be expressed as[34] $S^z=\sum_{m=-S}^{S} mY^{mm}$, $S^+=\sum_{m=-S}^{S} C_m^+ Y^{m+1,m}$, and $S^-=\sum_{m=-S}^{S} C_m^- Y^{m-1,m}$, with S representing the large spin quantum number and $Y^{m,n}=|Sm\rangle\langle Sn|$. Hence, the total Hamilton is rewritten as

$$\begin{aligned} H &= \sum_{k,\alpha,\sigma} \varepsilon_{k\alpha} c_{k\alpha\sigma}^\dagger c_{k\alpha\sigma} \\ &+ \sum_{k,\alpha,\sigma} (t_{k\alpha} c_{k\alpha\sigma}^\dagger X^{0\sigma} + H.c.) + \sum_{\sigma=\uparrow,\downarrow} \varepsilon_0 X^{\sigma\sigma} \\ &- \frac{J_\parallel}{2} \sum_{m=-S}^{S} m(X^{\uparrow\uparrow} - X^{\downarrow\downarrow}) Y^{mm} \\ &- \frac{J_\perp}{2} \sum_{m=-S}^{S} (C_m^- X^{\uparrow\downarrow} Y^{m-1,m} + C_m^+ X^{\downarrow\uparrow} Y^{m+1,m}). \end{aligned} \tag{2}$$

The retarded Green's function $G_\sigma^r(\omega) \equiv \langle\langle c_\sigma | c_\sigma^\dagger \rangle\rangle^r$, which will be needed in the density of states $\rho_\sigma = -(1/\pi) Im G_\sigma^r(\omega)$ and transport calculations, is expressed as

$$G_\sigma^r(\omega) = \langle\langle X^{0\sigma} | c_\sigma^\dagger \rangle\rangle^r = \sum_m \langle\langle X^{0\sigma} Y^{mm} | c_\sigma^\dagger \rangle\rangle^r. \tag{3}$$

We use the equation of motion method to calculate the retarded Green's function. Although the equation of motion method is an approximate one due to truncation scheme, it was shown that this method can capture qualitatively the Kondo physics[48]. The equation of motion of $\langle\langle X^{0\sigma} Y^{mm} | c_\sigma^\dagger \rangle\rangle^r$ reads

$$\left(\omega-\varepsilon_0+\delta_\sigma\frac{J_\parallel}{2}m\right)\langle\langle X^{0\sigma}Y^{mm}|c_\sigma^\dagger\rangle\rangle^r = P_{0m}+P_{\sigma m}-\frac{J_\perp}{2}C_{m\pm1}^{\mp}\langle\langle X^{0\overline{\sigma}}Y^{m,m\pm1}|c_\sigma^\dagger\rangle\rangle^r + \sum_{k\alpha}t_{k\alpha}^*\langle\langle(X^{00}+X^{\sigma\sigma})c_{k\alpha\sigma}Y^{mm}|c_\sigma^\dagger\rangle\rangle^r + \sum_{k\alpha}t_{k\alpha}^*\langle\langle X^{\overline{\sigma}\sigma}c_{k\alpha\overline{\sigma}}Y^{mm}|c_\sigma^\dagger\rangle\rangle^r, \tag{4}$$

where the upper (lower) sign applies for $\sigma=\uparrow(\downarrow)$. The averages are defined as $P_{0m}\equiv\langle X^{00}Y^{mm}\rangle$, $P_{\sigma m}\equiv\langle X^{\sigma\sigma}Y^{mm}\rangle$. One may notice that in the above equation there is a newly generated Green's function $\langle\langle X^{0\overline{\sigma}}Y^{m,m\pm1}|c_\sigma^\dagger\rangle\rangle^r$ that has the same order as $\langle\langle X^{0\sigma}Y^{mm}|c_\sigma^\dagger\rangle\rangle^r$. Other newly generated Green's functions are high-order ones that contain just one lead-operator. The equation of motion of these high-order Green's functions will generate higher-order ones containing two lead-operators. Here is an example:

$$\begin{aligned}(\omega-\varepsilon_{k\alpha})\langle\langle X^{00}c_{k\alpha\sigma}Y^{mm}|c_\sigma^\dagger\rangle\rangle^r &= \langle X^{\sigma0}c_{k\alpha\sigma}Y^{mm}\rangle \\ &-\sum_{k'\alpha'}t_{k'\alpha'}\langle\langle c_{k'\alpha'\sigma}^\dagger c_{k\alpha\sigma}X^{0\sigma}Y^{mm}|c_\sigma^\dagger\rangle\rangle^r \\ &-\sum_{k'\alpha'}t_{k'\alpha'}\langle\langle c_{k'\alpha'\overline{\sigma}}^\dagger c_{k\alpha\sigma}X^{0\overline{\sigma}}Y^{mm}|c_\sigma^\dagger\rangle\rangle^r \\ &-\sum_{k'\alpha'}t_{k'\alpha'}^*\langle\langle c_{k'\alpha'\sigma}c_{k\alpha\sigma}X^{\sigma0}Y^{mm}|c_\sigma^\dagger\rangle\rangle^r \\ &-\sum_{k'\alpha'}t_{k'\alpha'}^*\langle\langle c_{k'\alpha'\overline{\sigma}}c_{k\alpha\sigma}X^{\overline{\sigma}0}Y^{mm}|c_\sigma^\dagger\rangle\rangle^r \\ &+t_{k\alpha}\langle\langle X^{0\sigma}Y^{mm}|c_\sigma^\dagger\rangle\rangle^r.\end{aligned} \tag{5}$$

We truncate these higher-order Green's functions following the procedure proposed by Meir, Wingreen, and Lee[5], in which we pull the operator pair of leads out of the Green's functions and regard them as an average. This truncation approximation captures Kondo physics well when the temperature of the system is low.

After this truncation, Eq. (5) becomes

$$\begin{aligned}(\omega-\varepsilon_{k\alpha})\langle\langle X^{00}c_{k\alpha\sigma}Y^{mm}|c_\sigma^\dagger\rangle\rangle^r &= -t_{k\alpha}f_\alpha(\varepsilon_k)\langle\langle X^{0\sigma}Y^{mm}|c_\sigma^\dagger\rangle\rangle^r \\ &+t_{k\alpha}\langle\langle X^{0\sigma}Y^{mm}|c_\sigma^\dagger\rangle\rangle^r,\end{aligned} \tag{6}$$

in which the average $\langle X^{\sigma0}c_{k\alpha\sigma}Y^{mm}\rangle$ is simply discarded, $f_\alpha(\varepsilon_k)=\langle c_{k\alpha\sigma}^\dagger c_{k\alpha\sigma}\rangle$ is the Fermi function, and other averages of lead operator pairs equal zero.

In the same way, one can obtain the equation of motion of $\langle\langle X^{\sigma\sigma}c_{k\alpha\sigma}Y^{mm}|c_\sigma^\dagger\rangle\rangle^r$, which couples with the other three high-order Green's functions $\langle\langle X^{\sigma\overline{\sigma}}c_{k\alpha\sigma}Y^{mm+1}|c_\sigma^\dagger\rangle\rangle^r$, $\langle\langle X^{\overline{\sigma}\sigma}c_{k\alpha\sigma}Y^{m+1m}|c_\sigma^\dagger\rangle\rangle^r$ and $\langle\langle X^{\overline{\sigma}\overline{\sigma}}c_{k\alpha\sigma}Y^{m+1m+1}|c_\sigma^\dagger\rangle\rangle^r$. In the calculation procedure, one may notice that the high-order Green's functions containing one operator $c_{k\alpha\sigma}$ couple each other, while the high-order Green's functions with $c_{k\alpha\overline{\sigma}}$ couple each other. These are $\langle\langle X^{\overline{\sigma}\sigma}c_{k\alpha\overline{\sigma}}Y^{mm}|c_\sigma^\dagger\rangle\rangle^r$, $\langle\langle X^{\sigma\sigma}c_{k\alpha\overline{\sigma}}Y^{m-1m}|c_\sigma^\dagger\rangle\rangle^r$, $\langle\langle X^{\overline{\sigma}\overline{\sigma}}c_{k\alpha\overline{\sigma}}Y^{mm+1}|c_\sigma^\dagger\rangle\rangle^r$, and $\langle\langle X^{\sigma\overline{\sigma}}c_{k\alpha\sigma}Y^{m-1m+1}|c_{\overline{\sigma}}^\dagger\rangle\rangle^r$. After solving these simultaneous equations, we get the solutions of these one-lead-operator Green's functions. Inserting them back into Eq. (4) and the equation of motion of $\langle\langle X^{0\overline{\sigma}}Y^{m,m\pm1}|c_\sigma^\dagger\rangle\rangle^r$, we get the analytical results of the retarded dot Green's function

$$\langle\langle X^{0\sigma}Y^{mm}|c_\sigma^\dagger\rangle\rangle^r = \frac{\left[\omega-\varepsilon_0-\frac{J_\parallel}{2}(\delta_\sigma m+1)+\Sigma_d^\sigma\right](P_{0m}+P_{\sigma m})}{\det M_\sigma} - \frac{\left(\frac{J_\perp}{2}C_m^\pm+\Sigma_b^\sigma\right)\langle X^{\sigma\overline{\sigma}}Y^{m,m\pm1}\rangle}{\det M_\sigma}, \tag{7}$$

where the matrix M_σ is defined as

$$M_\sigma=\begin{bmatrix}M_{11} & M_{12}\\ M_{21} & M_{22}\end{bmatrix}, \tag{8}$$

with $M_{11}=\omega-\varepsilon_0+\delta_\sigma mJ_\parallel/2+\Sigma_a^\sigma$ $M_{12}=J_\perp C_m^\pm/2+\Sigma_b^\sigma$ $M_{21}=J_\perp C_m^\pm/2+\Sigma_c^\sigma$ and $M_{22}=\omega-\varepsilon_0-(\delta_\sigma m+1)J_\parallel/2+\Sigma_d^\sigma$.

This analytical expression for the retarded Green's function is one of the main results in this work, and it is the starting point for further numerical discussions. In Eq. (7), $\langle X^{\sigma\overline{\sigma}}Y^{m,m\pm1}\rangle$ is an average appearing in the equation of motion of $\langle\langle X^{0\overline{\sigma}}Y^{m,m\pm1}|c_\sigma^\dagger\rangle\rangle^r$. One may notice that this average has a self-adjoint average, $\langle X^{\overline{\sigma}\sigma}Y^{m\pm1,m}\rangle$. In Green's function theory, the averages can be related with Green's functions via the fluctuation-dissipation theorem $\langle AB\rangle=-(1/\pi)\int d\omega f(\omega)Im\langle\langle B|A\rangle\rangle^r$, in which $f(\omega)$ is the Fermi function. If considering the non-equilibrium situation, one can simply impose bias onto the Fermi function of this theorem, i.e., $f(\omega)\to\overline{f}(\omega)=[f_L(\omega)\Gamma_L+f_R(\omega)\Gamma_R]/(\Gamma_L+\Gamma_R)$. In order to relate the averages (P_{0m}, $P_{\sigma m}$, $\langle X^{\sigma\overline{\sigma}}Y^{m,m\pm1}\rangle$,

and $\langle X^{\bar{\sigma}\sigma}Y^{m\pm1,m}\rangle$) with Green's functions, one may find that the Green's functions $\langle\langle X^{0\sigma}Y^{mm}|c_\sigma^\dagger\rangle\rangle^r$, $\langle\langle X^{0\bar{\sigma}}Y^{m,m\pm1}|c_\sigma^\dagger\rangle\rangle^r$, $\langle\langle X^{0\sigma}Y^{mm}|X^{\bar{0}0}Y^{m\pm1,m}\rangle\rangle^r$, and $\langle\langle X^{0\bar{\sigma}}Y^{m,m\pm1}|X^{\bar{0}0}Y^{m\pm1,m}\rangle\rangle^r$ are useful. In Eqs. (7) and (8) $\Sigma^\sigma_{a,b,c,d}$ are combinations of Kondo self-energies that characterize the low-temperature Kondo transport properties of the dot. The Kondo self-energies are given as follows

$$\Sigma_1(\omega)=\sum_{k\alpha}\frac{|t_{k\alpha}|^2 f_{k\alpha}}{\omega-\varepsilon_{k\alpha}}, \tag{9}$$

$$\Sigma_1^{a\pm}(\omega,m)=\sum_{k\alpha}\frac{|t_{k\alpha}|^2 f_{k\alpha}}{\omega-\varepsilon_{k\alpha}\pm 2\Delta E\left(m+\frac{1}{2}\right)}, \tag{10}$$

$$\Sigma_1^{b\pm}(\omega,m)=\sum_{k\alpha}\frac{|t_{k\alpha}|^2 f_{k\alpha}}{\omega-\varepsilon_{k\alpha}\pm \Delta_1(m)}, \tag{11}$$

$$\Sigma_1^{c\pm}(\omega,m)=\sum_{k\alpha}\frac{|t_{k\alpha}|^2 f_{k\alpha}}{\omega-\varepsilon_{k\alpha}\pm \Delta_2(m)}, \tag{12}$$

where $\Delta_{1,2}$ are defined as

$$\Delta_1(m)\equiv\Delta E\left(m+\frac{1}{2}\right)+\Delta E\left(-m+\frac{1}{2}\right), \tag{13}$$

$$\Delta_2(m)\equiv\Delta E\left(m+\frac{1}{2}\right)-\Delta E\left(-m+\frac{1}{2}\right). \tag{14}$$

In principle, in Eqs. (9)–(12) at the pole positions of the self-energies, the Kondo peaks should manifest themselves in density of states and conductance. However, at the same time, these self-energies are modulated by parameters of the system. For example, $\Sigma_a^\uparrow$ is a combination of Kondo self-energies:

$$\begin{aligned}\Sigma_a^\uparrow(\omega,m)\;=\;&\Sigma_1(1-\Omega)-\Sigma_0-\Sigma_1^{a+}\frac{1-\Omega}{2}-\Sigma_1^{a-}\frac{1-\Omega}{2}\\&-\Sigma_1^{b-}\Lambda_\uparrow^{b-}-\Sigma_1^{c-}\Lambda_\uparrow^{c-}-\Sigma_1^{b+}\Lambda_\uparrow^{b+}-\Sigma_1^{c+}\Lambda_\uparrow^{c+},\end{aligned} \tag{15}$$

where the coefficients $\Omega(m)$ and $\Lambda_\uparrow^{b-}(m)$ (as examples) are defined as

$$\Omega(m)=\frac{\left(\frac{J_\perp}{2}C_m^+\right)^2}{2\Delta E^2\left(m+\frac{1}{2}\right)}+\frac{\left[\frac{J_\parallel}{2}(2m+1)\right]^2}{4\Delta E^2\left(m+\frac{1}{2}\right)}, \tag{16}$$

and

$$\begin{aligned}\Lambda_\uparrow^{b-}(m)\;=\;&\left[\Delta_1^2(m)-mJ_\parallel\Delta_1(m)-Q^2(m)+\frac{J_\parallel}{2}\frac{R^2(m)}{\Delta_2(m)}\right]\\&/8\Delta E\left(m+\frac{1}{2}\right)\Delta E\left(-m+\frac{1}{2}\right),\end{aligned} \tag{17}$$

where $R^2(m)\equiv(J_\perp C_m^+/2)^2-(J_\perp C_m^-/2)^2+2m(J_\parallel/2)^2$ and $Q^2(m)\equiv(J_\perp C_m^+/2)^2+(J_\perp C_m^-/2)^2+(J_\parallel/2)^2$ are defined for conciseness. These coefficients are dimensionless combinations of the anisotropy parameters $J_\parallel$ and $J_\perp$.

References

1. Kondo, J. Resistance minimus in dilute magnetic alloys. *Prog. Theor. Phys.* **32,** 37 (1964).
2. Schrieffer, J. R. & Wolff, P. A. Relation between the anderson and kondo hamiltonians. *Phys. Rev.* **149,** 491 (1966).
3. Wilson, K. G. The renormalization group: Critical phenomena and the kondo problem. *Phys. Rev.* **47,** 773 (1975).
4. Cronenwett, S. M., Oosterkamp, T. H. & Kouwenhoven, L. P. A tunable kondo effect in quantum dots. *Science* (Washington, DC, US) **281,** 540 (1998).
5. Meir, Y., Wingreen, N. S. & Lee, P. A. Low-temperature transport throuth a quantum dot: The anderson model out of equilibrium. *Phys. Rev. Lett.* **70,** 2601 (1993).
6. Martinek, J. *et al.* Kondo effect in quantum dots coupled to ferromagnetic leads. *Phys. Rev. Lett.* **91,** 127203 (2003).
7. Martinek, J. *et al.* Gate-controlled spin splitting in quantum dots with ferromagnetic leads in the kondo regime. *Phys. Rev. B* **72,** 121302 (2005).
8. Yuan, M. *et al.* Signatures of the valley kondo effect in si/sige quantum dots. *Phys. Rev. B* **90,** 035302 (2014).
9. Gr¨uner, G. & Zawadowski, A. Theory of tunneling centers in metallic systems: Role of excited states and orbital kondo effect. *Phys. Rev. Lett.* **72,** 542 (1994).
10. Kuemmeth, F. *et al.* Coupling of spin and orbital motion of electrons in carbon nanotubes. *Nature* (London) **452,** 448 (2008).

11. Fang, T.-F., Zuo, W. & H.-G., L. Kondo effect in carbon nanotube quantum dots with spin-orbit coupling. *Phys. Rev. Lett.* **101,** 246805 (2008).
12. Chiolero, A. & Loss, D. Macroscopic quantum coherence in molecular magnets. *Phys. Rev. Lett.* **80,** 169 (1998).
13. Liu, J. *et al.* Quantum step heights in hysteresis loops of molecular magnets. *Phys. Rev. B* **65,** 224401 (2002).
14. Heersche, H. B. *et al.* Electron transport through single mn12 molecular magnets. *Phys. Rev. Lett.* **96,** 206801 (2006).
15. Romeike, C. *et al.* Quantum-tunneling-induced kondo effect in single molecular magnets. *Phys. Rev. Lett.* **96,** 196601 (2006).
16. Leuenberger, M. N. & Mucciolo, E. R. Berry-phase oscillations of the kondo effect in single-molecule magnets. *Phys. Rev. Lett.* **97,** 126601 (2006).
17. Romeike, C. *et al.* Kondo-transport spectroscopy of single molecule magnets. *Phys. Rev. Lett.* **97,** 206601 (2006).
18. Misiorny, M. & Barna's, J. Magnetic switching of a single molecular magnet due to spin-polarized current. *Phys. Rev. B* **75,** 134425 (2007).
19. Trif, M. *et al.* Spin-electric coupling in molecular magnets. *Phys. Rev. Lett.* **101,** 217201 (2008).
20. Hackl, A. *et al.* Nonequilibrium spin dynamics in the ferromagnetic kondo model. *Phys. Rev. Lett.* **102,** 196601 (2009).
21. Wang, R. Q. *et al.* Thermoelectric effect in single-molecule-magnet junctions. *Phys. Rev. Lett.* **105,** 057202 (2010).
22. Misiorny, M., Weymann, I. & Barnaś, J. Interplay of the kondo effect and spin-polarized transport in magnetic molecules, adatoms, and quantum dots. *Phys. Rev. Lett.* **106,** 126602 (2011).
23. Stadler, P., Holmqvist, C. & Belzig, W. Josephson current through a quantum dot coupled to a molecular magnet. *Phys. Rev. B* **88,** 104512 (2013).
24. Elste, F. & Timm, C. Resonant and kondo tunneling through molecular magnets. *Phys. Rev. B* **81,** 024421 (2010).
25. Tolea, M. & Buł ka, B. R. Theoretical study of electronic transport through a small quantum dot with a magnetic impurity. *Phys. Rev. B* **75,** 125301 (2007).
26. Kawahara, S. L. *et al.* Kondo peak splitting on a single adatom coupled to a magnetic cluster. *Phys. Rev. B* **82,** 020406(R) (2010).
27. Kubo, T., Tokura, Y. & Tarucha, S. Exotic pseudospin Kondo effect in laterally coupled double quantum dots. *Phys. Rev. B* **77,** 041305(R) (2008).
28. Sasaki, S., Tamura, H., Akazaki, T. & Fujisawa, T. Fano-Kondo Interplay in a Side-Coupled Double Quantum Dot. *Phys. Rev. Lett.* **103,** 266806 (2009).
29. Eichler, A., Weiss, M. & Schonenberger, C. Gate-tunable split Kondo effect in a carbon nanotube quantum dot. *Nanotechnology* **22,** 265204 (2011).
30. Ferreira, I. L., Orellana, P. A., Martins, G. B., Souza, F. M. & Vernek, E. Capacitively coupled double quantum dot system in the Kondo regime. *Phys. Rev. B* **84,** 205320 (2011).
31. Jabben, T., Grewe, N. & Schmitt, S. Spectral properties of the two-impurity Anderson model with varying distance and various interactions. *Phys. Rev. B* **85,** 045133 (2012).
32. Crisan, M., Grosu, I. & Tifrea, I. An equation of motion analysis of the two stage Kondo effect in T-shaped double-quantum-dot systems. *Physica E* **66,** 245 (2015).
33. Wojcik, K. P. & Weymann, I. Two-stage Kondo effect in T-shaped double quantum dots with ferromagnetic leads. *Phys. Rev. B* **91,** 134422 (2015).
34. Niu, P.-B. *et al.* Quantum transport through anisotropic molecular magnets: Hubbard green function approach. *Phys. Lett. A* **376,** 1481 (2012).
35. Besombes, L. *et al.* Probing the spin state of a single magnetic ion in an individual quantum dot. *Phys. Rev.* **93,** 207403 (2004).
36. Leger, Y. *et al.* Geometrical effects on the optical properties of quantum dots doped with a single magnetic atom. *Phys. Rev. Lett.* **95,** 047403 (2005).
37. Leger, Y. *et al.* Electrical control of a single mn atom in a quantum dot. *Phys. Rev. Lett.* **97,** 107401 (2006).
38. Le Gall, C. *et al.* Optical spin orientation of a single manganese atom in a semiconductor quantum dot using quasiresonant photoexcitation. *Phys. Rev. Lett.* **102,** 127402 (2009).
39. Fernandez-Rossier, J. & Aguado, R. Mn-doped ii-vi quantum dots: artificial molecular magnets. *Phys. Status Solidi C* **3,** 3734 (2006).
40. Fernandez-Rossier, J. & Aguado, R. Single-electron transport in electrically tunable nanomagnets. *Phys. Rev. Lett.* **98,** 106805 (2007).
41. Contreras-Pulido, L. D. & Aguado, R. Shot noise spectrum of artificial single-molecule magnets: Measuring spin relaxation times via the dicke effect. *Phys. Rev. B* **81,** 161309(R) (2010).
42. Meir, Y. & Wingreen, N. S. Landauer formula for the current through an interacting electron region. *Phys. Rev. Lett.* **68,** 2512 (1992).
43. Haug, H. J. W. & Jauho, A.-P. *Quantum kinetics in transport and optics of semiconductors*. (Berlin, Springer) (2008).
44. Haldane, F. D. M. Scaling Theory of the Asymmetric Anderson Model. *Phys. Rev. Lett.* **40,** 416 (1978).
45. Hewson, A. C. *The Kondo problem to heavy fermions*. (Cambridge University Press) (1993).
46. Misiorny, M., Weymann, I. & Barnaś, J. Influence of magnetic anisotropy on the Kondo effect and spin-polarized transport through magnetic molecules, adatoms, and quantum dots. *Phys. Rev. B* **84,** 035445 (2011).
47. Theumann, A. Self-consistent solution of the anderson model. *Phys. Rev*. **178,** 978 (1969).
48. Lacroix, C. Density of states for the anderson model. *J. Phys. F: Metal Phys*. **11,** 2389 (1981).
49. Luo, H.-G., Ying, Z. J. & Wang, S. J. Equation of motion approach to the solution of the anderson model. *Phys. Rev. B* **59,** 9710 (1999).
50. Świrkowicz, R., Barnaś, J. & Wilczyński, M. Nonequilibrium kondo effect in quantum dots. *Phys. Rev. B* **68,** 195318 (2003).
51. Andersen, B. M. *et al.* Nonequilibrium transport through a spinful quantum dot with superconducting leads. *Phys. Rev. Lett.* **107,** 256802 (2011).
52. Niu, P.-B., Wang, Q. & Nie, Y.-H. Transport through artificial single-molecule magnets: Spin-pair state sequential tunneling and kondo effects. *Chin. Phys. B* **22,** 027307 (2013).
53. Niu, P.-B. *et al.* Inelastic low-temperature transport through a quantum dot with a mn ion. *Journal of Magnetism and Magnetic Materials* **324,** 2324 (2012).
54. Luo, B. *et al.* Ultrahigh spin thermopower and pure spin current in a single-molecule magnet. *Sci. Rep*. **4,** 4128 (2014).

Acknowledgements

This work was supported by the National Natural Science Foundation of China (Grant nos. 11504210, 11504211, 11504212, 11274207, 11274208, 11174115, 11325417, 11547108), Key Program of Ministry of Education of China (Grant no. 212018), Shanxi Provincial scientific and technological project (2015031002-2), Shanxi Provincial Natural Science Foundation (Grant nos. 2013011007-2, 2013021010-5), and Outstanding Innovative Teams of Higher Learning Institutions of Shanxi Province.

Author Contributions

H.G.L. put forwards the idea and supervised the whole work. P.N. performed the numerical calculations and wrote the manuscript. Y.L. and Z.S. entered the discussions and analyzed the results. Y.H.N. revised the manuscript. All authors reviewed the manuscript.

Additional Information

Competing financial interests: The authors declare no competing financial interests.

How to cite this article: Niu, P. *et al.* Kondo peak splitting and Kondo dip induced by a local moment. *Sci. Rep.* **5**, 18021; doi: 10.1038/srep18021 (2015).